American Mineralogist, Volume 73, pages 105–118, 1988

Polytypism in micas: A polyhedral approach to energy calculations

Richard N. Abbott, Jr.
Department of Geology, Appalachian State University, Boone, North Carolina 28608, U.S.A.
Charles W. Burnham
Department of Earth and Planetary Sciences, Harvard University, Cambridge, Massachusetts 02138, U.S.A.

Abstract

There has been wide speculation about the structural factors responsible for the observed frequency of the different mica polytypes. The purpose of this investigation is to identify the important factors and to test the relevant ones by using calculated cohesive energies to discriminate between alternative model structures. Sets of structures were constructed, based on talc, pyrophyllite, muscovite, biotite, and anandite. Each model set was specifically designed so that all structures in a given set would have essentially the same short-range repulsive forces and essentially the same van der Waals forces. The difference between the cohesive energies of two structures could then be ascribed essentially entirely to long-range Coulomb electrostatic forces. The method is a natural extension of the polyhedral approach to crystal chemistry.

Of the various parameters designed to characterize deviations from structural ideality, only Δz and α are specifically related to the articulation of the various coordination polyhedra. Other parameters measure the departure from ideal geometry of individual coordination polyhedra. We identify Δz as the best parameter for predicting the stable polytype. Most micas with Δz less than 0.1 Å are *1M* polytypes, regardless of composition and other structural parameters. Most micas with Δz greater than 0.1 Å are $2M_1$ polytypes regardless of composition and other structural parameters. The conspicuous exceptions include the lithian micas and the brittle mica anandite, $[Ba(Mg,Fe)_3(Si_3Fe)O_{10}(OH)S]$. Though significantly variable, α bears no apparent relationship to the stability of the *1M* versus the $2M_1$ polytype.

The calculations support both theoretical and empirical observations regarding (a) the predominance of *1M* and $2M_1$ polytypes and (b) the scarcity of $2M_2$ and *2O* polytypes. Al-Si "disordering" in micas is subject to certain rules: (a) the principle of aluminum avoidance and (b) the same ratio of Al to Si in all tetrahedral sheets. The relative positioning of tetrahedral Al cations on opposite sides of the octahedral sheet seems not to be important. For muscovite-$2M_1$, there are at least 48 crystal-chemically reasonable Al-Si orderings with very nearly the same low energy. The different orderings should be more or less equally represented in actual structures. Calculated energies are most sensitive to *inter*layer Al-Al separations. In *1M* and $2M_1$ polytypes, Al-Si orderings consistent with a 2_1 axis parallel to *b* are especially favorable.

Introduction

There are fundamental differences in the unit-layer structures of dioctahedral and trioctahedral micas (Bailey, 1984). The differences are in some combination responsible for the general observation that most dioctahedral micas are $2M_1$ polytypes, using the notation of Ramsdell (1947), whereas most trioctahedral micas are *1M* (Bailey, 1984). Other simple polytypes—$2M_2$, *2O*, *3T*, and *6H* (Smith and Yoder, 1956)—are comparatively rare or largely restricted to special compositions; for instance, anandite $[Ba(Mg,Fe)_3(Si_3Fe)O_{10}(OH)S]$, which is a *2O* brittle mica, and the lithian micas, many of which are *3T* or $2M_2$ polytypes (Bailey, 1984). Although there are excellent crystal-chemical grounds for understanding the scarcity of $2M_2$, *2O*, and *6H* polytypes (Radoslovich, 1959, 1960; Güven, 1971; Thompson, 1981), there is little consensus and much speculation (Güven, 1971; Bailey, 1984) regarding the structural factors responsible for the overwhelming predominance of $2M_1$-dioctahedral and *1M*-trioctahedral micas.

The purpose of this research is to identify the relevant structural factors controlling mica polytypism and to test the important ones by comparing calculated cohesive energies for appropriate model structures. Although the primary goal is a better understanding of polytypism, this end is not achieved without paying considerable attention to short-range ordering of tetrahedral cations (Abbott, 1984; Abbott et al., 1986). The calculations help to iden-

0003–004X/88/0102–0105$02.00

TABLE 1. Structural parameters of trioctahedral and dioctahedral micas

	Ideal	Trioctahedral (24 structures)	Dioctahedral (22 structures)
Avg. $\overline{T–O}$ (Å)	—	1.66(0.01)	1.64(0.02)
Avg. τ (°)	109.5	110.5(0.5)	111.0(0.8)
Avg. $\overline{M1–O}$ (Å)	—	2.08(0.02)	2.21(0.06)
Avg. ψ(M1) (°)	54.75	58.9(0.6)	61(1)
Avg. $\overline{M2–O}$ (Å)	—	2.08(0.02)	1.95(0.04)
Avg. ψ(M2) (°)	54.75	58.8(0.6)	57.0(0.4)
Avg. α (°)	0	6(3)	11(4)
Avg. Δz (Å)	0	0.02(0.02)	0.18(0.06)
Avg. s	−0.333	−0.333(0.004)	−0.37(0.01)

Note: The table includes only nongermanian, nonlithian, and nonbrittle trioctahedral and dioctahedral micas from Bailey (1984). Values in parentheses represent one standard deviation.

tify the direct and indirect influences on polytypism of the following factors: (1) OH ⇌ F exchange, (2) Al-Si ordering, and (3) M1 ⇌ vacancy exchange (trioctahedral vs. dioctahedral structures).

RELEVANT STRUCTURAL PARAMETERS

The differences in unit-layer structures of dioctahedral and trioctahedral micas can be quantified, for the purpose of comparison, in a number of ways. Several of the standard parameters for 69 structural determinations of dioctahedral and trioctahedral micas have been compiled by Bailey (1984). The parameters for 14 brittle micas have been compiled by Guggenheim (1984). The parameters measure the departure of a given structure from ideality (Pauling, 1930; Jackson and West, 1930; Gruner, 1934; Pabst, 1955). Table 1 presents the statistics on the structural parameters for 46 nonlithian and nongermanian micas from Bailey (1984). The parameters are explained in Figure 1 and include (1) the tetrahedral rotation, α ($0° < \alpha < 30°$), (2) the O_{basal}–T–O_{apical} bond angle, τ ($\tau_{ideal} = 109°28'$), (3) an angular measure of octahedral flattening, ψ ($\psi_{ideal} = 54°44'$), (4) the interlayer tetrahedral shift, s (approximately $0.333a$), and (5) a measure of departure from coplanarity of the basal oxygens, $\Delta z = [z(O_{basal})_{max} - z(O_{basal})_{min}][c \sin \beta]$, (0 Å $< \Delta z <$ 0.35 Å). Essentially, Δz measures the amplitude of corrugations in the surface defined by the basal oxygens. In Table 1 we have also included statistics on the important mean bond lengths, $\overline{T–O}$, $\overline{M1–O}$, and $\overline{M2–O}$.

Most of the parameters—$\overline{T–O}$, τ, $\overline{M–O}$ (M = M1 or M2), ψ, and s—are specifically related to the geometries of individual coordination polyhedra. These parameters are strongly dependent on cation substitution, hence on bulk composition. The mean $\overline{T–O}$ distance, for instance, is a measure of the ratio of Al to Si (Smith, 1954; Baur, 1970; Hazen and Burnham, 1973). The similarity in the averages of the $\overline{T–O}$ distances for the dioctahedral and trioctahedral micas simply reflects the common ratio of Al to Si (approx. ⅓). The value of τ is essentially the same for dioctahedral and trioctahedral micas by virtue of the inherent rigidity and incompressibility (Hazen and Finger, 1982; Hazen, 1985) of Si and Al tetrahedra. The averages of the $\overline{M–O}$ distances are different for dioctahedral and trioctahedral micas, but this is merely a reflection of the size of the common M substituents, M2 = Al and M1 = vacancy in the former versus M1 = M2 = Mg or Fe^{2+} in the latter. The average values for ψ (M1 or M2) are directly proportional to the averages of the $\overline{M–O}$ distances (M = M1 or M2). The tetrahedral shift, s, is greater in the dioctahedral micas than in the trioctahedral micas because the disparity in the sizes of the M1 (= vacant) and M2 coordination polyhedra is greater in the former than in the latter.

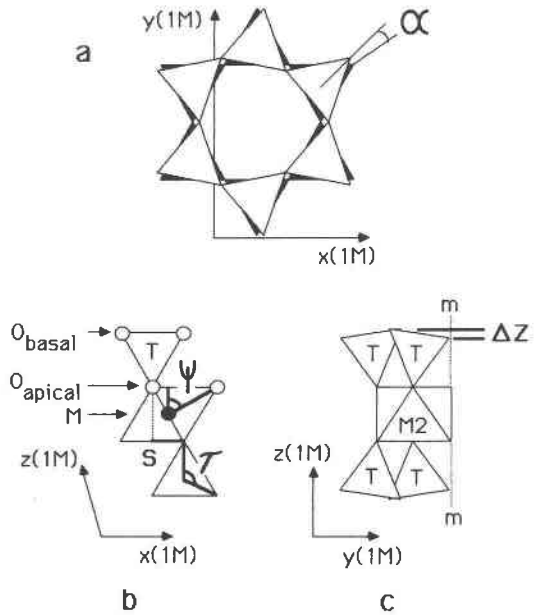

Fig. 1. Structural parameters. (a) Projection of tetrahedral sheet onto (001). The shaded tetrahedra are in the ideal configuration ($\alpha = 0$). The symmetry of the sheet is 6 mm. Solid outlined tetrahedra are rotated through the angle α. The symmetry of the tetrahedral sheet is reduced to $3m$. (b) Projection of part of a unit layer onto *1M* setting (010), looking down the unit layer diad. The following sites are indicated: T = tetrahedral site, M = octahedral site, O_{basal} = basal oxygen, O_{apical} = apical oxygen. The following structural parameters are indicated: the O_{basal}–T–O_{apical} angle, τ; the octahedral flattening angle, ψ; and the tetrahedral shift, s. (c) View of portion of unit-layer structure, looking down *1M* setting a axis. The parameter Δz is indicated.

Unlike the other parameters in Table 1, α and Δz are direct measures of the manner of articulation of the various coordination polyhedra. Both parameters are sensitive to variations in the other parameters. Hence, they happen to be distinctly different in the dioctahedral and trioctahedral micas, but only because of the differences in the common M1 and M2 substituents. Because they are not specifically related to the geometries of individual polyhedra, but rather to the way the polyhedra are connected, α and Δz share certain advantages in identifying causes underlying the obvious correlation between the

polytype and the occupancy of the octahedral sites (Table 1):

1. The value of α is independent of structural variations due to homogeneous size-scaling. Two structures that are distinguishable on the basis of $\overline{T–O}$ and $\overline{M–O}$ values may be the same in other respects if the ratios of $\overline{T–O}$ to $\overline{M1–O}$ and $\overline{M2–O}$ are the same in the two structures. One structure is simply homogeneously bigger than the other. Problems associated with size-scaling of this sort may be more insidiously embedded in the complex chemistries and structures of micas than might otherwise be indicated by a simple inspection of $\overline{T–O}$ and $\overline{M–O}$ distances. For this reason, we have avoided the size-dependent parameters, such as $\overline{T–O}$ and $\overline{M–O}$, in order to avoid false or ambiguous conclusions based on distinctions between structures, or parts thereof, that differ only in size-scaling.

2. Though Δz does vary in response to homogeneous size-scaling because it is a function of $c \sin \beta$, the dependency is small. This can be seen when it is considered that the percent variation in Δz, as measured for instance by $100\sigma/\Delta z_{mean}$, where σ = the standard deviation of the $z(O_{basal})$ values, is very much greater than the anticipated percent variation in $(c \sin \beta)/n$ (= 10 Å), where n is the number of unit layers in one c translation, i.e., $n = 1$ for the *1M* polytype, $n = 2$ for $2M_1$, etc. Consequently, variations in Δz are largely independent of variations due to homogeneous size-scaling. A better definition for Δz might be $n[z(O_{basal})_{max} - z(O_{basal})_{min}]$, which would be truly independent of homogeneous size-scaling. However, we have elected to retain the original formulation of Δz for the sake of comparison with other investigations.

3. Finally, it should be noted that Δz and α are significantly more variable than any of the other parameters, both within and between the major dioctahedral and trioctahedral groupings.

Figure 2 is a plot of α and Δz for the nonlithian micas from Bailey (1984) and Guggenheim (1984). The trioctahedral micas are plotted as solid symbols; the dioctahedral micas, as open symbols. The shape of the symbol indicates the polytype. Specific chemical traits are keyed by number to individual symbols wherever a coherent group, such as the paragonites, could not be encircled conveniently. The group marked Ge includes synthetic germanian micas in which Ge has been substituted for Si. The data points marked T&R (Takeda and Ross, 1975), R&R (Richardson and Richardson, 1982), talc, pyrophyllite, and 4 (anandite), are the bases for model structures used in our energy calculations. The following features should be noted: (1) Most of the trioctahedral micas are *1M* polytypes. (2) Most of the dioctahedral micas are $2M_1$ polytypes. (3) With two exceptions (phengites), the *1M* micas are restricted to low values of Δz (less than approximately 0.10 Å). (4) With three exceptions, the $2M_1$ micas are restricted to high values of Δz (greater than approximately 0.10 Å). (5) The dioctahedral mica celadonite, with a low Δz, is a *1M* polytype. (6) The trioctahedral mica clintonite, with a high Δz, is a $2M_1$ polytype. But the structure (Akhundov et al., 1961) was very poorly refined (final $R = \sim 19.5\%$) and may be discredited. Material from the same locality has since been shown to be disordered with only a statistical tendency toward $2M_1$ stacking (Bailey, pers. comm., 1987). (7) Except for anandite, the tetrahedral rotation (α) bears no obvious relationship to the polytype. (8) The combination of high Δz and low α may be crucial in stabilizing the *2O* polytype. (9) The brittle micas have extreme values for α. The margarites and two of the clintonites have the highest α values, and the polytype, $2M_1$ and *1M*, respectively, depends on Δz in a manner that is consistent with the potassiun micas. At the other extreme, anandites have very low α values. (10) There are *1M*-trioctahedral Ba-rich micas with low Δz values. Thus, the Ba in anandite is not necessarily responsible for the *2O* stacking.

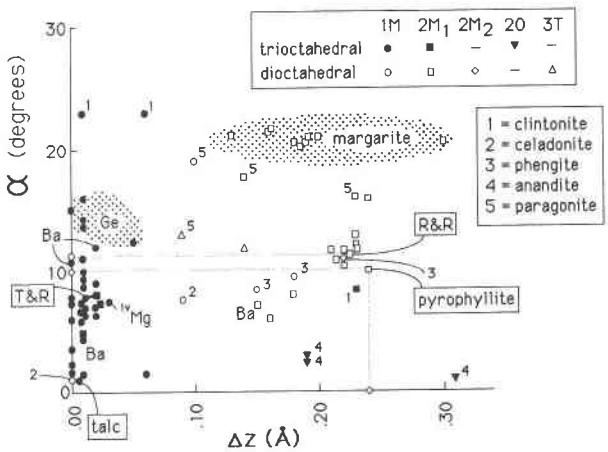

Fig. 2. Plot of α vs. Δz for nonlithian micas culled from Bailey (1984) and Guggenheim (1984). R&R = Richardson and Richardson (1982), T&R = Takeda and Ross (1975), talc = Rayner and Brown (1973), pyrophyllite = Lee and Guggenheim (1981).

With regard to the relative stability of *1M* and $2M_1$ polytypes, Δz is the single most important parameter of those listed in Table 1 and in Bailey's (1984) and Guggenheim's (1984) more detailed tabulations. We recognize three kinds of corrugations:

1. Pure corrugations. This type of distortion complements a vacancy in the M1 site and, hence, is prominent in dioctahedral micas. Pure distortions may also occur in trioctahedral micas in conjunction with the ordering of very different cations on the M1 and M2 sites, such as in the trioctahedral lithian micas (Bailey, 1984). Pure corrugations, as defined here, have nothing to do with cation substitution on tetrahedral sites. Effects due to pure corrugations may, however, be difficult to separate from effects due to cation substitutions on the tetrahedral sites. Certainty that corrugations are pure, therefore, exists only in talc, pyrophyllite, celadonite, or other micas with no substitution on the tetrahedral sites.

2. Ordered substitutional corrugations. Individual and mean bond lengths for tetrahedrally coordinated Al are substantially longer than for tetrahedrally coordinated Si

(Smith, 1954; Baur, 1970; Hazen and Burnham, 1973). Thus, among other changes in a mica structure, the substitution of Al for Si produces differences in the z coordinates of the basal oxygens. If there is short-range Al-Si ordering, the resulting distortions may be modulated so as to produce coherent corrugations. Substitutional and pure corrugations may be involved in simple constructive or destructive interference, or some complex combination of these. The possible effects of such interferences are an interesting subject for speculation, but lie beyond the immediate concerns of this investigation.

Margarite represents a special case. In margarite there is a strict alternation of Al and Si tetrahedra (Guggenheim and Bailey, 1975) in accordance with Loewenstein's (1954) principle of aluminum avoidance. Each basal oxygen is shared equally between one Al and one Si such that the position of each basal oxygen is influenced equally by the two cations. Consequently, the corrugations, which are significant (Fig. 2), must be regarded as pure.

3. Random (disordered) substitutional distortions. The observed space group of muscovite-$2M_1$, $C2/c$, permits at least partial ordering of Al and Si on the tetrahedral sites. Yet there is no evidence for long-range ordering of any kind (Bailey, 1975, 1984). We will address this problem in more detail in subsequent sections. On the average, the two distinct tetrahedral sites in $C2/c$ muscovites are populated by the same ⅓ ratio of Al/Si. The reported Δz values measure a pure distortion, but for an average structure, possibly giving a false impression of the actual shape of the surface defined by the basal oxygens. If there is short-range ordering, the basal oxygens may be modulated in small domains, perhaps in a manner that is contrary to that suggested by the measured Δz for the average structure. On the other hand, if there is not even short-range ordering, Δz for the average structure may measure the only systematic disturbance of the surface defined by the basal oxygens—a systematic disturbance superimposed on random substitutional effects.

In this study, a great deal of effort was devoted to sorting out the relative importance of pure corrugations versus substitutional effects. This end was achieved by varying the relevant parameters in the following model structures and discriminating between the alternative structures on the basis of calculated cohesive energies.

Test structures

Five unit-layer structures, and modifications thereof, were tested in two or more of the four polytypic configurations: $1M$, $2M_1$, $2M_2$, and $2O$. The unit-layer models were derived from well-refined structure determinations on natural specimens: talc (Rayner and Brown, 1973), pyrophyllite (Lee and Guggenheim, 1981), biotite (Takeda and Ross, 1975), muscovite (Richardson and Richardson, 1982), and anandite (Filut et al., 1985). Table 2 lists unit-cell dimensions, mean bond lengths, and relevant structural parameters for the model structures. With the exception of pyrophyllite and talc, the parameters correspond essentially to those for the experimental structural determinations. The unit-layer structures for both talc and pyrophyllite were idealized slightly to conform with $1M$-$C2/m$ symmetry. The actual structures are triclinic in one-layer (10-Å) polytypes that defy description according to conventional stacking theories (Smith and Yoder, 1956; Thompson, 1981). Unlike true micas, in talc and pyrophyllite, the basal oxygens in the top of one layer are juxtaposed with those in the bottom of the next layer in such a way that the cations of the respective tetrahedral sheets do not superimpose when projected down c^*. Nonetheless, the observed unit-layer structures for both talc and pyrophyllite are very close to the slightly modified $C2/m$ structures for the parameters reported in Table 2. In the hypothetical model structures, adjacent sheets of basal oxygens were positioned as they are in micas.

None of the structure determinations provided coordinates for H. Initially, this problem was avoided by considering the OH to be replaced by F, thus neglecting influences of OH dipoles. Most of the models were tested as F-micas. Later on, further work was deemed unwise without taking into account the influences of OH bonds, whose orientations are so very different in trioctahedral and dioctahedral micas (Bassett, 1960; Giese, 1984). A series of OH model structures was manufactured in accordance with the findings of Giese (1984) regarding the length and orientation of the OH bond. For both trioctahedral and dioctahedral model structures, the OH bond length was fixed at 0.9 Å. In the former, the bond was oriented perpendicular to (001) and directed away from the plane of the octahedral cations. In the latter, the OH bond was oriented in the unit-layer mirror plane [i.e., (010) in $1M$ and $2O$, (110) in $2M_1$, and $(1,\bar{1},0)$ in $2M_2$] and inclined 12° from (001).

The structure determinations by Takeda and Ross (1975) are unique in providing the only direct comparison between naturally coexisting $1M$ and $2M_1$ micas. Among other observations, they showed that the two polytypes have virtually the same composition and unit-layer structure. In this case alone, there was no need to construct one or more hypothetical polytypes from the unit-layer structure of one real polytype. Energy calculations were performed on the actual structures.

For muscovite, a hypothetical $1M$ polytype was derived by transformation of the unit-cell geometry and atomic coordinates from the initial $2M_1$ structure of Table 2. The initial $2M_1$ atomic coordinates were very slightly modified to conform with $C2/m$ unit-layer symmetry. This was necessary in order to insure a unique mapping of the atomic coordinates from the $2M_1$ unit-cell orientation to the $1M$ unit-cell orientation.

Hypothetical $2O$, $2M_1$, and $2M_2$ polytypes were fashioned using the initial $C2/m$ unit-layer structures of both talc and pyrophyllite (Table 2). Only the hypothetical $1M$ polytype was constructed from the initial $2O$ anandite structure (Table 2).

Table 3 reports the real and hypothetical models tested in the investigation. Each row in Table 3 represents a

TABLE 2. Structural parameters and lattice geometries of model structures

	Ideal	Talc	Biotite		Pyrophyllite	Muscovite	Anandite
		C2/m	*C2/m*	*C2/c*	*C2/m*	*C2/c*	*Pnmn*
a (Å)	—	5.293	5.331	5.329	5.160	5.199	5.439
b (Å)	$a\sqrt{3}$	9.179	9.231	9.234	8.966	9.027	9.509
c (Å)	—	9.499	10.173	20.098	9.334	20.106	19.878
β (°)	—	100	100.16	95.09	100	95.78	90
$\overline{T1–O}$ (Å)	—	1.622	1.659	1.657	1.617	1.643	1.620
τ(T1) (°)	109.5	109.16	110.4	110.3	109.4	111.0	112.5
$\overline{T2–O}$ (Å)	—	—	—	1.662	—	1.643	1.799
τ(T2) (°)	109.5	—	—	110.2	—	111.0	112.6
α (°)	0	1	7.6	7.7	10.2	11.0	0.9
Δz (Å)	0	0.01	0.01	0.02	0.24	0.22	0.30
s	±0.333	−0.324	−0.335	−0.334	−0.383	+0.378	±0.337
$\overline{M1–O}$ (Å)	—	2.067	2.086	2.086	—	(2.253)*	2.097
ψ(M1) (°)	54.75	57.97	59.2	59.2	—	(61.7)*	59.8
$\overline{M2–O}$ (Å)	—	2.076	2.086	2.068	1.912	1.940	2.236
ψ(M2) (°)	54.75	58.09	58.9	58.9	57.1	56.6	55.3
$\overline{M3–O}$ (Å)							2.228
ψ(M3) (°)							55.2
$\overline{M4–O}$ (Å)							2.120
ψ(M4) (°)							60.2

* M1–O and ψ(M1) relative to center of M1 (vacancy).

model set, all of whose members have essentially the same unit-layer structure, at least within the limitations of (1) polytype-imposed symmetry differences and (2), where relevant, Al-Si ordering differences. Each entry in Table 3 under the different polytype headings is the number of distinct Al-Si (Fe-Si, in the case of anandite) ordered structures that were constructed for the corresponding polytype. The rationale for the limited choice of Al(Fe)-Si orderings (in contrast to Giese, 1984) is presented in the next section. For pyrophyllite and talc models, the tetrahedral sheets are pure Si_2O_5; hence one structure per polytype in each model set is sufficient. For the model sets labeled DLS in Table 3, Si–O and Al–O (or ^{iv}Fe–O) bond lengths were adjusted by distance–least-squares analysis (Baerlocher et al., 1977). The details of the DLS calculations are described in a later section. The Al(^{iv}Fe)-Si orderings for the polytypes of the *non-DLS* model sets are distinguishable from one another only on the basis of charge distribution. For instance, in each *1M* structure of the non-DLS OH-biotite model set, the atomic coordinates conform to *C2/m,* whereas the charge distribution (owing to the ordering of Al and Si) is in a lower-order space group ($P2_1$, $P2$, $P\bar{1}$, and $P;\bar{1}'$; see Abbott, 1984). For each structure in the DLS-adjusted OH-biotite model set, both the charge distribution and the atomic coordinates have the same reduced symmetry.

The corrugations were removed from some model sets by setting the z coordinate of each basal oxygen to the average of the z values in the actual corrugated strucure. One model set for OH-pyrophyllite ($\alpha = 0$) was constructed with the tetrahedral rotation (α) set to zero.

Ordering of tetrahedral cations

The important observed space groups for biotite (*C2/c* in $2M_1$ and *C2/m* in *1M*), muscovite-$2M_1$ (*C2/c*), and anandite-*2O* (*Pnmn*) permit partial (*C2/c, Pnmn*) or no (*C2/m*) ordering of tetrahedral cations. In muscovite-$2M_1$ and biotite-$2M_1$, where limited ordering is possible, the structural determinations (Richardson and Richardson, 1982; Takeda and Ross, 1975) indicate that Al and Si are essentially completely disordered. The structure of anandite (Filut et al., 1985) indicates that ^{iv}Fe and one-third

TABLE 3. Model sets on which energy calculations were performed

End member	Model characteristics	*1M*	*2O*	$2M_1$	$2M_2$
		Biotite model sets*			
F		**4**	—	8	—
OH		**4**	—	8	—
OH	DLS	**4**	—	8	—
		Muscovite model sets*			
F		4	—	**8**	—
OH		4	—	**8**	—
OH	$\Delta z = 0$	**4**	—	8	—
OH	DLS	4	—	**12**	—
		Pyrophyllite model sets			
F		1	—	**1**	—
F	$\Delta z = 0$	**1**	—	1	—
OH		1	1	**1**	1
OH	$\Delta z = 0$	**1**	—	1	—
OH	$\alpha = 0$	1	**1**	1	**1**
		Talc model sets			
F		**1**	—	1	—
F	$\Delta z = 0$	**1**	—	1	—
OH		**1**	1	1	1
OH	$\Delta z = 0$	**1**	—	1	—
		Anandite model sets			
OH		**2**	4	—	—
OH	DLS	2	**4**	—	—

Note: Number of Al-Si (Fe-Si in the case of anandite) orderings. Boldface values indicate lowest-energy polytype.

* Results reported earlier (Abbott et al., 1986) and only summarized here.

of the Si are disordered on one of the two distinct sites ($T2 = Fe_{1/2}Si_{1/2}$), with the remainder of the Si on the other site (T1 = Si). As we already noted, Bailey (1975, 1984) has argued that there is no evidence for long-range ordering in either the $2M_1$ or the *1M* polytypes of muscovite or biotite, even when the structures are reconsidered in reduced-symmetry space groups. Recent nuclear magnetic resonance studies (Sanz and Serratosa, 1984; Sanz et al., 1986; Herrero et al., 1985; Herrero, 1987) indicate a somewhat ill-defined short-range ordering that does, however, comply with Loewenstein's (1954) principle of aluminum avoidance. Other workers (Gatineau, 1964; Gatineau and Mering, 1966; Abbott, 1984) have postulated models for short-range ordering, based on X-ray or electron diffraction observations. Abbott et al. (1986) have considered the consequences and energetics of short-range ordering of tetrahedral cations. The problem of disordering versus short- or long-range ordering is crucial to the calculation of realistic cohesive energies.

The cohesive energy of a structure depends on nearest-neighbor forces (Burnham, 1985). In the ionic modeling approach, these forces make sense only in the context of individual sites in a structure being occupied by discrete atoms (i.e., T = Si or Al) and not by hybrid atoms (e.g., $T = Al_{1/4}Si_{3/4}$) (Giese, 1984; Burnham, 1985). Presumably, the real structure consists of a Boltzmann distribution of differently ordered unit cells. At present, the problem can be accommodated only crudely by three approaches:

1. Consider all possible ordering schemes. Even in seemingly simple cases, this can lead to an overwhelming number of structures. The problem becomes intractable, and for this reason alone, the approach has enjoyed little, if any, popularity.

2. Select, at random, a manageable subset of structures from the total number of possibilities. This approach has been used with some measure of success by Giese (1984, 1986) who selected 100 Al-Si ordered muscovite structures from 1820 possibilities and 100 margarite structures from 12 870 possibilities. The procedure has at least one serious flaw in cases where only one or two particularly favorable structures exist out of hundreds of possibilities, as in the case of margarite (Giese, 1984). In such cases, the one or more exceptional cases may be overlooked, if they cannot be anticipated a priori. In the case of margarite (Giese, 1984), the one favorable structure could be anticipated and was included in the set of structures tested. The approach does not discriminate between symmetrically equivalent structures, nor does it discriminate between crystal-chemically reasonable and unreasonable structures.

3. Use a set of ordered structures consisting of only symmetrically distinct arrangements that obey reasonable crystal-chemical principles. In their energy calculations concerning the relationship of Al-Si ordering to the position of Na in albite, by using symmetrically distinct Al-Si orderings that obey Loewenstein's (1954) principle of aluminum avoidance, Post and Burnham (1987) limited the number of orderings from 1820 to 56. The approach is justified because symmetrically equivalent orderings have the same energy, hence are redundant, and because crystal-chemically unreasonable structures will have high energies, hence correspondingly low representations according to Boltzmann's law.

We have adopted the third approach here, selecting only those Al-Si ordered structures that fulfill the following criteria:

1. For the muscovite and biotite model sets, each $2M_1$ and *1M* Al-Si ordered structure is symmetrically distinct under the space-group operations of $C2/c$ and $C2/m$, respectively. For the anandite model sets, each *2O* and *1M* Fe-Si–ordered structure is symmetrically distinct under the operations of *Pnmn* and $P2/m$, respectively.

2. All tetrahedral sheets in a given structure have the same ratio of Al to Si (Abbott, 1984; Abbott et al., 1986). This eliminates from consideration any subgroup of $C2/m$ containing the mirror plane or the *a*-glide plane and any subgroup of *Pnmn* containing the mirror plane. All model structures obey Loewenstein's (1954) principle of aluminum avoidance (Sanz and Serratosa, 1984; Sanz et al., 1986; Herrero et al., 1985; Herrero, 1987).

After screening the possibilities (28 for *1M*; 1820 for $2M_1$; 1820 for *2O*), there are only four symmetrically distinct and crystal-chemically reasonable *1M* ordered structures (Abbott, 1984), twelve $2M_1$ structures, and twelve *2O* structures. Only one of the $2M_1$ model subsets in Table 3 (DLS-adjusted OH-muscovite) includes all 12 of the Al-Si orderings. Each of the other muscovite and biotite model sets—created for an earlier study (Abbott et al., 1986)—includes only 8 of the 12 possibilities, though we are confident, on the basis of the $2M_1$ structure calculations on all 12, that our conclusions are unaffected by this earlier omission. Two of the 4 possible anandite-*1M* structures and 8 of the 12 possible anandite-*2O* structures were eliminated because they were not consistent with the observed (Filut et al., 1985) partial ordering of Fe and Si.

Each of the ordered structures can be characterized by a space group that is subordinate to the space group of the disordered or partially ordered structure. The space groups are reported in subsequent tables.

We have included tetrahedral-site orderings that violate what one of us (Abbott, 1984) has referred to as Güven's rule. Güven (1971) argued that two apical oxygens of Al tetrahedra forming the same shared octahedral edge should be especially unfavorable with respect to the local balancing of electrostatic charge. The rule refers to the situation where both of the tetrahedra in Figure 1b are occupied by Al. The sum of the Pauling (1960) bond strengths reaching each apical oxygen is 1.75. Thus, two electrostatically undersaturated oxygens are juxtaposed.

DLS analysis

The tetrahedral bond lengths for the hypothetically Al-Si ordered muscovite and biotite models (and Fe-Si ordered anandite models) were adjusted by distance–least-squares analysis, using the program DLS-76 (Baerlocher et

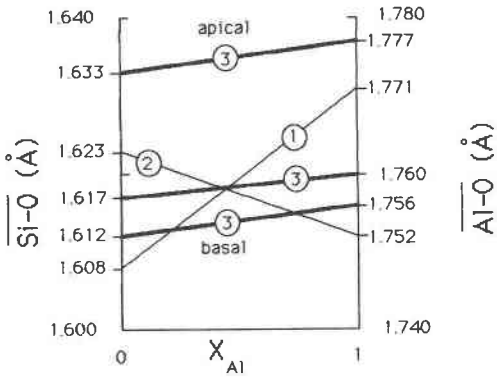

Fig. 3. T–O bond lengths as a function of X_{Al} = Al/(Si + Al). The heavy lines (marked 3) are based on the Si–O distances in pyrophyllite and the average of the slopes of the lines 1 and 2, which are due to Hazen and Burnham (1973) and Baur (1981), respectively. The lower and upper heavy lines correspond respectively to the variation in $\overline{T\text{–}O}_{basal}$ and $T\text{–}O_{apical}$. The middle heavy line is for the weighted mean $\overline{T\text{–}O}$ distance = $0.75(T\text{–}O_{basal}) + 0.25(T\text{–}O_{apical})$.

al., 1977; Villager, 1969). Only the atomic coordinates (x, y, z) for the basal oxygens and z coordinates for tetrahedral cations were allowed to vary. In the refinements, the O-O interactions were assigned $\frac{1}{10}$ of the weighting assigned to the T-O interactions. This weighting gave reasonable results and is consistent with weightings used elsewhere, as discussed by Burnham (1985).

The mean cation–oxygen bond length for a given tetrahedral site ($\overline{T\text{–}O}$) in any Al-Si mica can be used as a measure of the proportion of Al and Si on that site. Two algorithms (Fig. 3) are in common use for evaluating the fraction of Al, X_{Al} = Al/(Si + Al), on a given tetrahedral site: $\overline{T\text{–}O} = 1.608 + 0.163X_{Al}$ (Hazen and Burnham, 1973) and $\overline{T\text{–}O} = 1.623 + 0.129X_{Al}$ (Baur, 1981). In the present analysis we have formulated two new algorithms in order to treat the long $T\text{–}O_{apical}$ bond and the short $T\text{–}O_{basal}$ bonds separately.

The mean tetrahedral bond length in pyrophyllite (Lee and Guggenheim, 1981) is $\overline{Si\text{–}O}$ = 1.617 Å; it includes 3 × $Si\text{–}O_{basal}$ of 1.612 Å, and $Si\text{–}O_{apical}$ of 1.633 Å. Using these bond lengths and the average of the slopes (Fig. 3) determined by Hazen and Burnham (1973) and Baur (1981), we get

$$\overline{T\text{–}O}_{basal} = 1.612 + 0.142X_{Al}$$

and

$$T\text{–}O_{apical} = 1.633 + 0.144X_{Al}.$$

The mean $O_{basal}\text{–}O_{basal}$ and mean $O_{basal}\text{–}O_{apical}$ distances were scaled accordingly, relative to these distances in pyrophyllite. The relevant bond lengths prescribed for the DLS calculations are given in Table 4.

For anandite, the tetrahedral bond lengths were formulated by extrapolation from the dimensions of the pure Si–O tetrahedron, through the dimensions of the $Fe_{½}Si_{½}$ disordered tetrahedron, to the dimensions for the hypothetically pure Fe tetrahedron. In the extrapolation, a distinction was made among bonds involving different kinds of bridging oxygens, i.e., $Fe\text{–}O_{basal}\text{–}Si$ vs. $Si\text{–}O_{basal}\text{–}Si$. By this means, four kinds of $O_{basal}\text{–}O_{basal}$ and four kinds of $O_{basal}\text{–}O_{apical}$ bonds could be prescribed. The prescribed bond lengths are reported in Table 4. Note that, unlike the Al-Si micas, in anandite the $T\text{–}O_{apical}$ bonds are shorter than the $T\text{–}O_{basal}$ bonds (Filut et al., 1985).

TABLE 4. T–O bond lengths (Å) prescribed for DLS refinement

Muscovite and biotite			
$Si\text{–}O_{basal}$	1.612	$Al\text{–}O_{basal}$	1.754
$Si\text{–}O_{apical}$	1.633	$Al\text{–}O_{apical}$	1.777
$O_{apical}\text{–}O_{basal}$	2.648	$O_{apical}\text{–}O_{basal}$	2.882
$O_{basal}\text{–}O_{basal}$	2.628	$O_{basal}\text{–}O_{basal}$	2.860
Anandite			
$Si\text{–}O_{basal}$	1.623	$Fe\text{–}O_{basal}$	1.881
$Si\text{–}O_{apical}$	1.613	$Fe\text{–}O_{apical}$	1.857
$O_{apical}\text{–}O_{basal}$	2.689	$O_{apical}\text{–}O_{basal}$	3.107
	2.645		
	2.711	$O_{basal}\text{–}O_{basal}$	2.996
$O_{basal}\text{–}O_{basal}$	2.594		
	2.646		
	2.568		

Note: There are three distinct $O_{apical}\text{–}O_{basal}$ distances and three distinct $O_{basal}\text{–}O_{basal}$ distances for the Si tetrahedra.

The unit-cell dimensions of each polytype were not permitted to change during the course of DLS analysis. Changes in unit-cell geometry can be exaggerated in DLS analysis, leading to structures for which the calculated energies cannot be compared realistically. Unconstrained DLS analyses often lead to unrealistic changes in the articulation of the tetrahedral and octahedral coordination polyhedra. Even so, the conservative approach adopted here can lead to anomalous structures that are generally characterized by unrealistic A-site coordination polyhedra. Fortunately, the anomalous structures have correspondingly anomalous calculated energies and are therefore easily recognized. The DLS-adjusted *1M* modifications of OH-muscovite afford a good example. The unusually low calculated energies for the $P2_1$, $P\bar{1}$, and $P\bar{1}'$ structures—when compared with the energies for the various $2M_1$ structures—are due to unrealistically short K–O distances. The K polyhedra are not comparable in the *1M* and $2M_1$ structures. By way of contrast, the K polyhedra are essentially the same in the *1M* and $2M_1$ structures of each biotite model set because Δz is close to zero.

Energy calculations

If meaningful results are taken as an indication, there is reasonable justification for treating many silicate structures as ionic (Burnham, 1985). The proof of this rests essentially on the generally favorable comparison between properties calculated on the basis of the ionic model and measured properties. In the ionic model, there are

three important contributions to the cohesive energy, using the terminology of Burnham (1985): a long-range, or Coulomb, electrostatic term; a short-range repulsive term, and a van der Waals term. Of the several computer programs now available for calculating the cohesive energy, we used WMIN (Busing, 1981). In our calculations, we have included neither the short-range repulsive energy nor the van der Waals energy. We report only the Coulomb electrostatic energy. This simplification is justified in this study for the following reasons:

1. The models are based on the refined structures of naturally occurring minerals. We have assumed, a priori, that the structures represent equilibrium or, at the very least, near-equilibrium configurations. Under these circumstances, the absolute magnitude of the short-range repulsive energy is approximately 10% of the magnitude of the long-range Coulomb electrostatic energy (Giese, 1984), and the van der Waals energy is small.

2. Our structures were fashioned in such a way that the nearest-neighbor bonding relationships are, as nearly as possible, identical in all members of a given model set. This applies even to the DLS-adjusted structures. The essential differences between any two members of a given model set involve some combination of (a) the relative position of the Al(Fe)-Si ordered tetrahedral sheets on opposite sides of the octahedral sheet, (b) the manner of stacking successive layers (the polytype), and (c) the geometry of the interlayer-cation coordination polyhedron (K, Ba, vacancy). Under these circumstances, the short-range energy is essentially identical for all members of a model set, at least according to the currently available methods for evaluating the short-range energy (Burnham, 1985). It is therefore assumed that the differences in calculated energies correspond to structural differences for which the differences in short-range energy terms and van der Waals terms are negligible.

Because of the way we have constructed our model sets, the energy difference between two structures in the same model set is directly related to the manner of articulation of the different polyhedral units in the structures. The structures of a given model set may be thought of as being constructed from a fixed set of cation coordination polyhedra. In this sense, our calculations are a natural extension of Hazen's (1985; Hazen and Finger, 1982) "polyhedral approach to comparative crystal-chemistry."

Two notes of caution are in order: (1) We emphasize that any attempt to discriminate between different structures on the basis of calculated Coulomb electrostatic energies alone is meaningful only for members of the same model set. Structures from different model sets, differing in nearest-neighbor bonding relationships, cannot be compared realistically without taking into account both short-range and van der Waals interactions. (2) In some cases, the range of calculated energies for the members of a model set is exceedingly small in comparison with the absolute values. This raises the important question of the significance of differences that may amount to less than 1 in 7000 kJ. The reader should bear the following in mind: (a) The differences are anticipated to be small. This makes the method especially effective in identifying an unusual structure for which the energy deviates significantly from the mean. (b) The formulation for the Coulomb electrostatic energy is exact, and in principle the energy can be computed to any desired degree of precision. (c) The significance of the results is directly proportional to the care taken in the construction of the model structures. In the end, we point to the consistency of our results when compared with the natural states of micas and our expectations based on crystal-chemical principles.

Summary of previous results

Some of our results pertaining to biotite and muscovite have been reported elsewhere (Abbott et al., 1986). For the sake of comparison with the latest calculations, the findings of this earlier work are briefly summarized here: (1) For trioctahedral OH-micas (OH-biotite), the *1M* polytype is roughly 1.75 kJ/anion more stable than the $2M_1$ polytype. (2) For trioctahedral F-micas (F-biotite), the energy difference between the *1M* and $2M_1$ polytypes is about 91 kJ/anion in favor of *1M*. (3) For dioctahedral OH- and F-micas (OH- and F-muscovite), the $2M_1$ polytype is 1.2 to 2.1 kJ/anion more stable than *1M*. (4) For a given polytype and octahedral sheet structure, the various Al-Si orderings (with or without DLS refinement) have slightly different energies. (a) In $2M_1$ and *1M* polytypes of biotite or muscovite, the lowest-energy Al-Si orderings are consistently the ones with the most even distribution of tetrahedral Al atoms. That is, the most favorable orderings maximize the closest Al-Al separations. (b) In *1M* and $2M_1$ polytypes, Al-Si orderings consistent with a 2_1 axis parallel to *b* are especially favorable. The lowest-energy $2M_1$ orderings are in subgroups $P2_1/n$, $P2_1$, and $P2_1/c$; the lowest-energy *1M* ordering is in subgroup $P2_1$. On the other end of the spectrum, Al-Si orderings with a 2 axis parallel to *b* have by far the highest energies. (5) With the corrugations removed from the OH-muscovite ($\Delta z = 0$), there is essentially no energy difference between the lowest-energy Al-Si ordered $2M_1$ and *1M* polytypes.

New results and discussion

Pyrophyllite and talc. Table 5 reports the results of our calculations for talc and pyrophyllite. These model sets were prepared in order to examine the influence of pure distortions on stacking, without complications due to Al-Si substitutions.

The calculations on the various model sets for pyrophyllite indicate that $2M_1$ is the most stable polytype when $\Delta z \neq 0$ and $\alpha \neq 0$. The range of calculated energies in the unmodified OH model set spans a difference of 1.74 kJ/anion. Only the energies for the $2M_1$ and *2O* polytypes differ by more than one standard deviation ($\sigma = 0.7$ kJ/anion) from the mean energy (−7001.9 kJ/anion), such that $E_{2M_1} < E_{1M} < E_{2M_2} < E_{2O}$. It should be noted that the energy of the $2M_1$ polytype is only 0.11 kJ/anion less than that of the *1M* polytype. For F-pyrophyllite, the difference in the energies of the *1M* and $2M_1$ polytypes is

greater, approximately 0.56 kJ/anion, and still in favor of the latter polytype. When the structure is modified so that Δz is zero, the relative stability of the *1M* and $2M_1$ polytypes reverses, and the difference in the energies of the two polytypes increases to 1.36 kJ/anion for OH-pyrophyllite and 0.9 kJ/anion for F-pyrophyllite. This reversal shows the influence of pure corrugations in stabilizing the $2M_1$ polytype relative to the *1M* polytype. When the structure is modified so that α is zero, the relative stability of the various polytypes changes: $E_{2M_2} < E_{1M} < E_{2M_1} < E_{2O}$, favoring the $2M_2$ polytype. In the $\alpha = 0$ model set, only the $2M_2$ and *2O* polytypes have energies differing by more than 1 σ (0.7 kJ/anion) from the mean energy (−7052.0 kJ/anion). The high calculated energy for the *2O* polytype in the pyrophyllite model sets is consistent with the extreme scarcity (Bailey, 1984) of this polytype in nature.

Calculations on talc show that the four hypothetical polytypes have nearly the same energy, regardless of the differences between the model sets. For the unmodified OH-talc model set, the difference between the highest ($2M_1$) and lowest (*1M*) energies is only 0.1 kJ/anion, and all of the calculated energies lie within 1 σ (0.04 kJ/anion) of the mean (−6680.76 kJ/anion). The calculated energies for the *1M*, $2M_2$, and *2O* polytypes differ by less than 0.03 kJ/anion! The very small differences are obviously insignificant; the four polytypes are equally stable, hence equally likely. Alternatively, the layer-stacking scheme, if it obeys a Boltzmann distribution, would be random. It is interesting to note that when the structure is modified by setting Δz to zero (from the already low initial value of 0.005 Å), the difference in the energies of the $2M_1$ and *1M* polytypes increases slightly, giving a correspondingly slight preference (0.24–0.28 kJ/anion) to the *1M* polytype. This supports the observation (Fig. 2) that Δz is the important parameter with regard to the relative stability of the *1M* and $2M_1$ polytypes.

For both the OH-pyrophyllite structures and OH-talc structures, the relative order of the four polytypes is consistent with Thompson's (1981) suggestion that the geometry of the A-site coordination polyhedron (vacant in pyrophyllite and talc) is important in explaining the scarcity of the $2M_2$ and *2O* polytypes. When the tetrahedra are rotated ($\alpha > 0$) as in pyrophyllite, the coordination polyhedron for the A site is *trigonal antiprismatic* (octahedral) in the *1M* and $2M_1$ polytypes and *trigonal prismatic* in $2M_2$ and *2O* polytypes. Thompson (1981; Radoslovich, 1959, 1960; Güven, 1971) argued that the antiprismatic arrangement should be more stable, because interlayer O-O repulsions are less. Our calculations for the OH-pyrophyllites lend support on two accounts: (1) When $\alpha > 0$, the *2O* and $2M_2$ polytypes have significantly higher energies than either the *1M* or the $2M_1$ polytype. (2) When $\alpha = 0$, the order of stability of the polytypes changes such that the hypothetical $2M_2$ and *2O* polytypes have, respectively, the lowest and highest energies, thus emphasizing the importance of α rotation with regard to the stability (or instability) of the $2M_2$ and *2O* polytypes. When α and Δz are both close to zero, as in talc, the coordination polyhedron for the A site (vacant) is essentially hexagonal prismatic—the coordination number is 12 and essentially the same in all four polytypes. It follows that if the geometry of the A polyhedron alone determines the polytype, two possibilities may subtend: (1) The different polytypes should have the same frequency, or (2) the stacking sequence in a given structure should be random. In fact, neither possibility gains much support from natural examples (Fig. 2). Even among the low-α trioctahedral micas, the *1M* polytype seems to dominate.

That *2O* and $2M_2$ micas are indeed scarce in nature can surely be ascribed to the fact that most trioctahedral and dioctahedral micas have α values that differ significantly from zero (Fig. 2). Under these circumstances, the lowest-energy polytype is $2M_1$ or *1M*, depending on the presence or absence, respectively, of corrugations in the surface defined by the basal oxygens. It is interesting to note however that the three $2M_2$ lithian micas reported by Bailey (1984) all have α values around 5°, and the one phengite-$2M_2$ in Figure 2 has a value of α of approximately 11°! At present, we can only speculate about the causes for these anomalies.

The difference in the calculated energies for $2M_2$ and *2O* pyrophyllites (Table 5) deserves additional comment. In both of the model sets that include these polytypes, the $2M_2$ polytype has a significantly lower energy than the *2O* polytype. In the unmodified model set, the energy difference is 1.04 kJ/anion, whereas in the modified model set ($\alpha = 0$), the difference is approximately twice as great, 2.06 kJ/anion. This discrepancy might not otherwise command much attention if both polytypes had higher energies than either $2M_1$ or *1M* under all circumstances. But when $\alpha = 0$ and $\Delta z > 0$, the very low energy of the $2M_2$ polytype hints at a special structural problem. Figure 4a shows the A-site coordination polyhedron in the *2O* polytype under the conditions just stipulated, i.e., $\alpha = 0$ and $\Delta z > 0$. The polyhedron is an orthorhombic parallelepiped with edges parallel to the *2O a, b,* and *c* axes. Basal oxygens occupy the corners of the parallelepiped, and the A site is at the center. We shall refer to the O-O edge lengths as d_s (short), d_l (long), and d_z. The short edge in the (001) face, d_s, has a length equal to the shortest O_{basal}-O_{basal} distance. The edge length d_l equals $\sqrt{3}d_s$; and d_z, which is the shortest interlayer O-O separation, is approximately equal to d_s ($d_s \simeq d_z$). The trace of the unit-layer mirror plane is shown on the (001) faces of the polyhedron. The four shortest interlayer O-O distances have the same length, d_z. The next shortest interlayer distances are four in number, end-face diagonals each having length $\sqrt{(d_s^2 + d_z^2)}$. Other interlayer O-O distances are significantly longer. Figure 4b shows the A-site polyhedron for the $2M_2$ polytype under the same conditions, $\alpha = 0$ and $\Delta z > 0$. The polyhedron can be derived from the *2O* A-site polyhedron by rotating one of the (001) faces 60° about the normal to (001). The (001) faces have the same dimensions as in the *2O* polytype, d_s = (O-

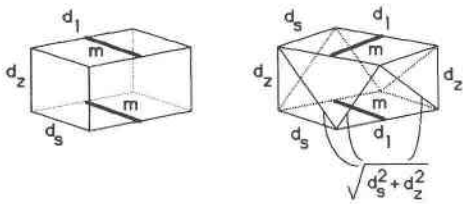

Fig. 4. A-site coordination polyhedron in (a) the *2O* polytype and (b) the $2M_2$ polytype, when $\Delta z > 0$, and $\alpha = 0$.

$O)_{basal}$ distance, and $d_l = \sqrt{3}d_s$. In the $2M_2$ polytype, the two shortest interlayer O-O separations are of length d_z. The next shortest interlayer O-O separations are six in number, each having length $\sqrt{(d_s^2 + d_z^2)}$. Other interlayer O-O distances are substantially longer. The eight A–O bond lengths are the same ($= \sqrt{5}d_s/2$) in both $2M_2$ and *2O* polytypes! Recalling that a Coulomb electrostatic repulsive force varies inversely with the square of the interatomic distance, the sum of the repulsions due to the eight shortest interlayer O-O distances would be approximately 20% more for the *2O* polytype than it would be for the $2M_2$ polytype. The $2M_2$ polytype should thus be more stable than the *2O* polytype. The argument is analogous to the one offered by Thompson (1981; Radoslovich, 1959, 1960, Güven, 1971) for the preference of trigonal *anti*prismatic (octahedral) coordination over trigonal prismatic coordination.

Anandite. Table 6 reports the results of our calculations on anandite. The first model set that we constructed was predicted on the basis that Fe and Si were disordered on one of the two crystallographically distinct tetrahedral sites, as indicated by the structure refinement (Filut et al., 1985). The average structure was treated as a fair representation of what would be, in this case, a special kind of substitutional distortion. The energies were calculated for different Fe^{3+}-Si charge-orderings in which the bond lengths were left unmodified by DLS. One of the *1M* structures has a significantly lower energy than any other structure. This suggests that the distortions represented by the average structure are not responsible for the observed *2O* polytype.

TABLE 6. Coulomb electrostatic energies for anandite, $Ba(Mg,Fe)_3(Si_3Fe^{3+})O_{10}(OH)S$

Polytype	Atomic coordinates	Charge distributions	Energy (kJ/anion)
	Non-DLS adjusted structure		
1M	*P2/m*	*P2*	−6038.87
1M	*P2/m*	*P*$\bar{1}$	**−6044.17**
2O	*Pnmn*	*Pn2n*	−6038.04
2O	*Pnmn*	$P2_122_1$	−6039.29
2O	*Pnmn*	$P2_1/n11$	−6035.00
2O	*Pnmn*	$P112_1/n$	−6039.05
	DLS-adjusted structures		
1M	*P2**		−6132.77
1M	*P*$\bar{1}$*		−6124.71
2O	*Pn2n**		**−6139.34**
2O	$P2_122_1$*		−6132.73
2O	$P2_1/n11$*		−6122.59
2O	$P112_1/n$*		**−6139.17**

Note: Boldface values indicate low-energy structures.
* Atomic coordinates and charge distribution are consistent with same space group.

In the second model set, the Si–O and Fe–O bond lengths were adjusted by DLS. For these calculations, two of the *2O* structures (*Pn2n* and $P112_1/n$) gave significantly lower energies than the other structures. This suggests that the actual structure may have short-range ordering, possibly consisting of domains of the crystallographically equivalent complexions (Abbott, 1984) of one or both of the low-energy configurations. The observed *2O* polytype appears to be stabilized by high Δz and low α in conjunction with distortions caused by Fe-Si ordering.

Muscovite. Table 7 and Figure 5 present our most recent calculations involving DLS-adjusted OH-muscovite structures. Of interest here are the very different characteristics of the results for the two polytypes, *1M* and $2M_1$. The anomalously low energies for three of the *1M* structures are due to unrealistically short DLS-modeled K–O distances. The K polyhedra are simply not comparable in the *1M* and $2M_1$ DLS-adjusted structures; hence the

TABLE 5. Coulomb electrostatic energies for pyrophyllite and talc model structures

End member	Model characteristics	Polytype energies (kJ/anion)			
		1M	*2O*	$2M_1$	$2M_2$
		Pyrophyllite model sets			
F		−6391.72	—	**−6392.28**	—
F	$\Delta z = 0$	**−6461.80**	—	−6460.90	—
OH		−7002.48	−7000.74	**−7002.59**	−7001.78
OH	$\Delta z = 0$	**−7069.36**	—	−7068.00	—
OH	$\alpha = 0$	−7052.24	−7050.98	−7051.89	**−7053.04**
		Talc model sets			
F		**−6094.76**	—	−6094.69	—
F	$\Delta z = 0$	**−6095.67**	—	−6095.43	—
OH		**−6680.80**	−6680.77	−6680.70	6680.77
OH	$\Delta z = 0$	**−6681.67**	—	−6681.39	—

Note: Boldface values indicate lowest-energy polytype.

TABLE 7. Coulomb electrostatic energies for muscovite

Structure	T-T′ = Al-Al′*	Energy (kJ/anion)	Mean
		Muscovite-*1M*	
$P2_1$†		−6689.73	−6600.12(126.91)
$P\bar{1}$†		−6646.35	
$P\bar{1}$‡		−6682.20	
P2‡		−6382.20	
		Muscovite-$2M_1$	
Pc†	31′	−6617.59	−6615.60(2.67)
Pn†	31′	−6613.47	
*P*2†	31′	−6613.23	
$P2_1$†	31′	−6618.15	
*P*2/*c*†	32′	−6612.85	−6615.64(2.79)
$P2_1/n$†	32′	−6618.43	
Pc‡	33′	−6613.72	−6616.82(1.81)
P*n*‡	33′	−6617.69	
*P*2‡	33′	−6617.55	
$P2_1$‡	33′	−6618.32	
$P2_1/c$‡	34′	−6618.08	−6615.15(2.96)
*P*2/*n*‡	34′	−6612.18	
		Intralayer relationships: muscovite-$2M_1$	
Structures that obey Güven's rule			−6615.64(2.24)
Structures that violate Güven's rule			−6616.26(2.41)
		Interlayer relationships: muscovite-$2M_1$	
Structures with *c* glide			−6615.57(2.30)
Structures with *n* glide			−6615.43(2.68)
Structures with 2 axis			−6613.96(2.13)
Structures with 2_1 axis			−6618.24(0.14)

Note: Values in parentheses represent one standard deviation.
* See Figure 5a.
† Structures that obey Güven's rule.
‡ Structures that violate Güven's rule.

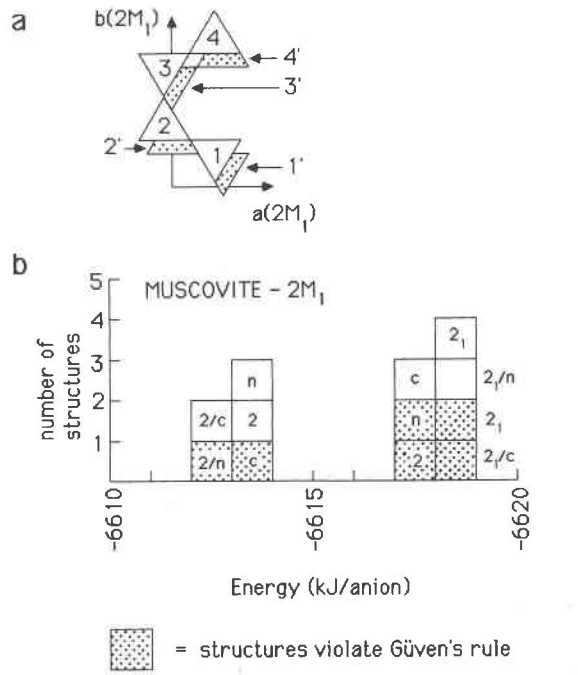

Fig. 5. (a) Labeling of tetrahedral sites in reference to Table 7. (b) Histogram of energies for 12 Al-Si orderings in muscovite-$2M_1$.

structures do not meet the criteria we have established for a valid comparison. The calculated energies cannot therefore be used as a reliable guide to the relative stability of the *1M* versus the $2M_1$ polytype. However, the K–O distances are similar in the four *1M* structures, so these structures constitute a valid set for comparing the effects of different Al-Si orderings. Likewise, the K–O distances are similar in the twelve $2M_1$ structures; hence they too constitute a valid set for comparison. Problems with the modeling of the A-site geometry were not encountered in the other model sets.

The energies for the four Al-Si ordered *1M* structures are very different (σ = 126.91 kJ/anion), with three structures ($P2_1$, $P\bar{1}$, $P\bar{1}'$) having the very lowest energies of all of the $2M_1$ and *1M* structures and the remaining *P*2 structure having the very highest energy. The Boltzmann distribution law would suggest that a hypothetical *1M* muscovite should be dominated by the $P2_1$, $P\bar{1}$, and $P\bar{1}'$ arrangements. The hypothetical structure would probably consist of small domains of the different Al-Si orderings and symmetrically equivalent orderings (Abbott, 1984), or it may consist of a mosaic of individual, differently ordered unit cells.

In contrast, the twelve $2M_1$ structures have very nearly the same energy (σ = 2.48 kJ/anion). The Boltzmann distribution law suggests that the different Al-Si orderings would be more or less equally represented. The actual energy would be close to the average, which just happens to be somewhat less than the average for the *1M* structures. That there are so many (12 plus symmetrically equivalent complexions, making 48 altogether) more or less equally accessible low-energy states suggests that it should be disordered (Giese, 1984). As for the *1M* polytype, a hypothetical, disordered muscovite-$2M_1$ may consist of small domains of the different Al-Si orderings (Abbott, 1984), or it may be a mosaic of individual, differently ordered unit cells.

On closer examination of Table 7, it becomes evident (Fig. 5) that there is a bimodal distribution of $2M_1$ energies. For this reason, it is instructive to sort the 12 structures into subsets, each being characterized by one or more common features. There are four distinct unit-layer structures, identified as 31′, 32′, 33′, and 34′. The designations refer to the Al-occupied sites as they are labeled in Figure 5a. Note that, within the limits of the standard deviation, the average energy is the same for each of the unit-layer groups. Evidently, the intralayer distribution of Al and Si (within the constraints set up earlier) has no bearing on the bimodal distribution of energies and, because the four unit-layer structures are very different (in terms of the relative positioning of the Al atoms), essentially no bearing on the preference for the $2M_1$ polytype. The 12 structures can be sorted in another way, according to elements of the space groups. In combinations or individually, the symmetry elements 2, 2_1, *c*, and *n* relate one unit layer to another and, hence, relate to the structure of the *inter*layer region. When sorted in this way (Table 7), the average energy and standard deviation for the group characterized by the 2_1 axis—space groups $P2_1/n$,

$P2_1$ (31′ or 33′), and $P2_1/c$—are substantially lower than the averages and standard deviations for the other groups. This indicates that layers related by 2_1 are particularly favorable. The group characterized by a 2-fold rotation has the highest average energy. Evidently, regardless of the unit-layer structure, relating adjacent layers by a 2-fold rotation is not a particularly good solution to the polytype problem. The calculations suggest (see Abbott et al., 1986) that a complex interplay between the unit-layer structure (i.e., Al-Si ordering) and structure of the interlayer region is responsible for stabilizing the $2M_1$ polytype.

Six of the $2M_1$ structures, corresponding to the 33′ and 34′ unit-layer structures—with double daggers in Table 7—violate Güven's (1971) rule. The average energy and standard deviation for this group are essentially the same as for the group that obeys Güven's rule (Table 7). Evidently, the influence of *intra*layer interactions involving tetrahedral Al polyhedra across the intervening octahedral sheet is minimal.

Structural determinations indicate that there is no long-range ordering of Al and Si in muscovite-$2M_1$ (Bailey, 1975, 1984). We suggest further that the disorder is not some manifestation of short-range ordering in small but discrete domains. As our calculations show, and as pointed out by Giese (1984, 1986), there are simply too many Al-Si orderings with nearly the same energy. However, we suggest that the disorder, real though it is on a unit-cell scale, is subject to certain rules: the principle of aluminum avoidance (Sanz and Serratosa, 1984; Sanz et al., 1986; Herrero et al., 1985; Herrero, 1987) and the same ratio of Al to Si in each sheet (Abbott, 1984). If this interpretation is correct, then by analogy with the pyrophyllite calculations, the preference of muscovite for $2M_1$ is probably a manifestation of pure distortion of the average structure, superimposed on disordered (but not completely random) substitutional distortions. This is in contrast to anandite, for which ordered substitutional distortions are implicated in the stabilization of the *2O* polytype. The *3T* polytype of muscovite, which is well-ordered with respect to Al and Si (Güven and Burnham, 1967), may be stabilized by the effects of ordered substitutional distortions.

Conclusions

1. F has a great influence in stabilizing the *1M* polytype in biotite, though the *1M* polytype is also favored for OH-biotite. F $\rightleftharpoons$ OH exchange has little or no influence in stabilizing the $2M_1$ polytype in dioctahedral micas (muscovite and pyrophyllite). Substitution of F for OH is thus much more important for biotites than it is for dioctahedral micas. Given the difference in the position of the H in dioctahedral versus trioctahedral layers, this makes sense because K^+-H^+ repulsion will be much greater in the latter. As would be expected, F has no special influence in stabilizing talc-*1M* because the A site is vacant.

2. Of the various parameters (Bailey, 1984) designed to characterize deviations from structural ideality, Δz has the most influence over the relative stability of *1M* and $2M_1$ polytypes. Most micas with Δz less than approximately 0.1 Å form *1M* polytypes, regardless of composition and other structural parameters. The *1M* polytype represents the default condition, for the absence of distortions except α rotation. Most micas with Δz greater than approximately 0.1 Å form $2M_1$ polytypes regardless of composition and other structural parameters. Conspicuous exceptions include the lithian micas and anandite.

3. Energy calculations for pyrophyllite, talc, muscovite, and biotite support the general observations regarding the stability of *1M* and $2M_1$ polytypes, and identify the most important kind of structural distortion to be pure corrugations in the surface defined by the basal oxygens—that is, corrugations directly related to the structure of the octahedral sheet, rather than corrugations due to substitutions within the tetrahedral sheets. Of course, corrugations of any kind in pyrophyllite and talc are pure. In muscovite and biotite, the distortions, as measured by Δz, can be thought of as pure corrugations, superimposed on disordered substitutional distortions. For anandite, the high Δz associated with the *2O* polytype seems to be a manifestation of ordered substitutional distortions in the tetrahedral sheets.

4. At high Δz, a low α in conjunction with pure distortions (hypothetical OH-pyrophyllite, $\alpha = 0$) stabilizes the $2M_2$ polytype, whereas a low α (less than approximately 3°) in conjunction with substitutional distortions (anandite) may stabilize the *2O* polytype.

5. The calculations on pyrophyllite and talc support Thompson's (1981; Radoslovich, 1959, 1960; Güven, 1971) proposal regarding the scarcity of $2M_2$ and *2O* polytypes for micas with rotated tetrahedra ($\alpha > 0$). This accounts for the vast majority of trioctahedral and dioctahedral micas (Fig. 2).

6. We suggest that the disordering of Al and Si in muscovite and biotite is subject to certain rules (Abbott, 1984; Abbott et al., 1986), chief among which are (a) the principle of aluminum avoidance (Sanz and Serratosa, 1984; Sanz et al., 1986; Herrero et al., 1985; Herrero, 1987) and (b) a constant ratio of Al to Si in all tetrahedral sheets (Abbott, 1984). On this basis, there are four crystal-chemically reasonable ordered unit-layer structures for *1M* and *2O* polytypes and four different ordered unit-layer structures for $2M_1$ and $2M_2$ polytypes. In a given biotite or muscovite model set, the lowest-energy Al-Si orderings are consistently the ones with the most evenly distributed tetrahedral Al. That is, the most favorable Al-Si orderings maximize the closest Al-Al separations. This is consistent with the findings of Sanz and Serratosa (1984), Sanz et al. (1986), Herrero et al. (1985), and Herrero (1987). In *1M* and $2M_1$ polytypes, Al-Si orderings consistent with a 2_1 axis parallel to *b* are especially favorable. The relationships are not as clearcut for hypothetical *1M*-dioctahedral structures, though the tendency appears to be the same.

7. We support Giese's (1984, 1986) explanation for the disordering of Al and Si in muscovite. There are many Al-Si ordering schemes with very nearly the same low energy. According to the Boltzmann distribution law, the different Al-Si arrangements would be more or less equally represented in the real structure.

8. Güven's (1971) rule concerning the relative positioning of tetrahedral Al atoms on opposite sides of the octahedral sheet does not seem to be important in the energetics of micas. By all indications the effect is minimal.

9. Energy calculations for the $2M_1$ DLS-adjusted OH-muscovite structures show that the ordering of Al and Si, subject to the constraints cited above, has little apparent influence on the energy attributable to the internal structure of the unit layer, but may have considerable influence on the energy attributable to the *inter*layer region. Hence, for $2M_1$ structures, the *inter*layer Al-Al separations are more important than the *intra*layer Al-Al separations. By analogy, the *inter*layer relationships in *1M* polytypes are probably more important than the *intra*layer relationships.

10. For the purpose of discriminating among the structures of a model set, as defined here, the use of the Coulomb electrostatic energy alone is justifiable. If a set of structures to be compared can be manufactured in such a way that the nearest-neighbor interatomic distances and bond angles are the same in all of the structures and hence the structures differ only in the articulation of a fixed set of polyhedral units, then the short-range repulsive energy and van der Waals energy will not vary significantly from one structure to another. Under these circumstances, differences in the cohesive energies will be due almost entirely to differences in the long-range Coulomb electrostatic interactions. The method is potentially very powerful in discriminating between structures that differ only in the ordering and articulation of a fixed set of polyhedral units. The effectiveness of the method depends on the strategy used in the design of the comparison and the skill in manufacturing the model sets. The approach is a natural extension of Hazen's (1985; Hazen and Finger, 1982) polyhedral approach to comparative crystal-chemistry.

Acknowledgments

Most of the calculations were performed on the geophysics computing facilities at Harvard University, during R.N.A.'s tenure as a postdoctoral fellow. The research was supported by NSF Grant EAR 79-20095 to C.W.B. We greatly appreciate the helpful comments of the reviewers, J. E. Post and S. W. Bailey.

References cited

Abbott, R.N., Jr. (1984) Al-Si ordering in 1M trioctahedral micas. Canadian Mineralogist, 22, 659–667.

Abbott, R.N., Jr., Burnham, C.W., and Post, J.E. (1986) Energetics of polytypism in di- and trioctahedral micas. International Mineralogical Association Abstracts with Program, 40.

Akhundov, Y.A., Mamedov, K.S., and Belov, N.V. (1961) The crystal structure of brandisite. Doklady Akademii Nauk SSSR, Earth Sciences, 137, 438–440.

Baerlocher, C., Hepp, A., and Meir, W.M. (1977) DLS-76: Program for the simulation of crystal structures. Institute of Crystallography and Petrography, ETH, Zurich, Switzerland.

Bailey, S.W. (1975) Cation ordering and pseudosymmetry in layer silicates. American Mineralogist, 60, 175–187.

———. (1984) Crystal chemistry of the micas. Mineralogical Society of America Reviews in Mineralogy, 13, 13–60.

Bassett, W.A. (1960) Role of hydroxyl orientation in mica alteration. Geological Society of America Bulletin, 71, 449.

Baur, W.H. (1970) Bond length variation and distorted coordination polyhedra in inorganic crystals. American Crystallographic Association Transactions, 6, 129–155.

———(1981) Interatomic distance predictions for computer simulation of crystal structures. In M. O'Keeffe and A. Navotsky, Eds., Structure and bonding in crystals, vol. II, p. 31–52. Academic Press, New York.

Burnham, C.W. (1985) Mineral structure energetics and modelling using the ionic approach. Mineralogical Society of America Reviews in Mineralogy, 14, 347–388.

Busing, W.R. (1981) WMIN: A computer program to model molecules and crystals in terms of potential energy functions. Oak Ridge National Laboratory, Special Paper ORNL-5747, 169 p.

Filut, M.A., Rule, A.L., and Bailey, S.W. (1985) Refinement of anandite-*2Or* structure. American Mineralogist, 70, 1298–1308.

Gatineau, P.L. (1964) Structure reelle de la muscovite. Repartition des substitutions isomorphiques. Bulletin de la Société Française de Minéralogie et de Cristallographie, 87, 321–355.

Gatineau, P.L., and Mering, J. (1966) Relations ordre-desordre dans les substitutions isomorphiques des micas. Centre National de la Recherche Scientifique, Groupe Français des Argiles, Bulletin, 18, 67–74.

Giese, R.F., Jr. (1984) Electrostatic energy models of micas. Mineralogical Society of America Reviews in Mineralogy, 13, 105–144.

———(1986) Detection of short-range order in substitutionally disordered cation sites of phyllosilicates. International Mineralogical Association Abstracts with Program, 111.

Gruner, J.W. (1934) The crystal structures of talc and pyrophyllite. Zeitschrift für Kristallographie, 88, 412–419.

Guggenheim, S. (1984) The brittle micas. Mineralogical Society of America Reviews in Mineralogy, 13, 61–104.

Guggenheim, S., and Bailey, S.W. (1975) Refinement of the margarite structure in subgroup symmetry. American Mineralogist, 60, 1023–1029.

Güven, N. (1971) Structural factors controlling stacking sequences in dioctahedral micas. Clays and Clay Minerals, 19, 159–165.

Güven, N., and Burnham, C.W. (1967) The crystal structure of 3T muscovite. Zeitschrift für Kristallographie, 125, 1–6.

Hazen, R.M. (1985) Comparative crystal chemistry and the polyhedral approach. Mineralogical Society of America Reviews in Mineralogy, 14, 317–346.

Hazen, R.M., and Burnham, C.W. (1973) The crystal structure of one-layer phlogopite and annite. American Mineralogist, 58, 889–900.

Hazen, R.M., and Finger, L.W. (1982) Comparative crystal chemistry. Wiley, New York.

Herrero, C.P. (1987) Monte Carlo simulation and calculation of electrostatic energies in the analyses of Si-Al distribution in micas. In L.G. Schultz, H. van Olphen, and F.A. Mumpton, Eds., Proceedings of the International Clay Conference, Denver, 1985, p. 24–30. Clay Mineral Society, Bloomington, Indiana.

Herrero, C.P., Sanz, J., and Serratosa, J.M. (1985) Tetrahedral cation ordering in layer silicates by ^{29}Si NMR spectroscopy. Solid State Communications, 53, 151–154.

Jackson, W.W., and West, J. (1930) The crystal structure of muscovite, $KAl_2(AlSi_3)O_{10}(OH)_2$. Zeitschrift für Kristallographie, 76, 211–227.

Lee, J.H., and Guggenheim, S. (1981) Single crystal X-ray refinement of pyrophyllite-*1Tc*. American Mineralogist, 66, 350–357.

Loewenstein, W. (1954) The distribution of aluminum in the tetrahedra of silicates and aluminates. American Mineralogist, 58, 92–96.

Pabst, A. (1955) Redescription of the single layer structure of the micas. American Mineralogist, 40, 967–974.

Pauling, L. (1930) The structure of the micas and related minerals. Proceedings of the National Academy of Science, 16, 123–129.

——— (1960) The nature of the chemical bond (3rd edition). Cornell University Press, Ithaca, New York.

Post, J.E., and Burnham, C.W. (1987) Structure-energy calculations on low and high albite. American Mineralogist, 72, 507–514.

Radoslovich, E.W. (1959) Structural control of polymorphism in micas. Nature, 183, 253.

——— (1960) The structure of muscovite, $KAl_2(Si_3Al)O_{10}(OH)_2$. Acta Crystallographica, 13, 919–932.

Ramsdell, L.S. (1947) Studies on silicon carbide. American Mineralogist, 32, 64–82.

Rayner, J.H., and Brown, G. (1973) The crystal structure of talc. Clays and Clay Minerals, 21, 103–114.

Richardson, S.M., and Richardson, J.W., Jr. (1982) Crystal structure of a pink muscovite from Archer's Post, Kenya: Implications for reverse pleochroism in dioctahedral micas. American Mineralogist, 67, 69–75.

Sanz, J., and Serratosa, J.M. (1984) ^{29}Si and ^{27}Al high-resolution MAS-NMR spectra of phyllosilicates. Journal of the American Chemical Society, 106, 4790–4793.

Sanz, J., Herrero, C.P., and Serratosa, J.M. (1986) Tetrahedral cation distribution in phyllosilicates 2:1 by ^{29}Si NMR spectroscopy. International Mineralogical Association Abstracts with Program, 220.

Smith, J.V. (1954) A review of the Al–O and Si–O distances. Acta Crystallographica, 13, 479.

Smith, J.V., and Yoder, H.S. (1956) Experimental and theoretical studies of mica polymorphs. Mineralogical Magazine, 31, 209–235.

Takeda, H., and Ross, M. (1975) Mica polytypism: Dissimilarities in the crystal structures of coexisting *1M* and *2M*$_1$ biotite. American Mineralogist, 60, 1030–1040.

Thompson, J.B., Jr. (1981) Polytypism in complex crystals: Contrasts between mica and classical polytypes. In M. O'Keeffe and A. Navrotsky, Eds., Structure and bonding in crystals, vol. II, p. 167–196. Academic Press, New York.

Villager, H. (1969) DLS manual. Institute for Crystallography and Petrography, ETH, Zurich, Switzerland.

MANUSCRIPT RECEIVED JULY 2, 1987
MANUSCRIPT ACCEPTED OCTOBER 9, 1987